Low-Temperature Pulsed EPR Study at 34 GHz of the Triplet States of the Primary Electron Donor P_{865} and the Carotenoid in Native and Mutant Bacterial Reaction Centers of *Rhodobacter sphaeroides*†

Aliaksandr Marchanka,‡ Mark Paddock,§ Wolfgang Lubitz,‡ and Maurice van Gastel*,‡

Max-Planck-Institut für Bioanorganische Chemie, P.O. Box 101365, D-45413 Mülheim an der Ruhr, Germany, and Department of Physics, University of California, San Diego, 9500 Gilman Drive, La Jolla, California 92093

Received August 8, 2007; Revised Manuscript Received October 17, 2007

ABSTRACT: The photosynthetic charge separation in bacterial reaction centers occurs predominantly along one of two nearly symmetric branches of cofactors. Low-temperature EPR spectra of the triplet states of the chlorophyll and carotenoid pigments in the reaction center of *Rhodobacter sphaeroides* R-26.1, 2.4.1 and two double-mutants GD(M203)/AW(M260) and LH(M214)/AW(M260) have been recorded at 34 GHz to investigate the relative activities of the "A" and "B" branches. The triplet states are found to derive from radical pair and intersystem crossing mechanisms, and the rates of formation are anisotropic. The former mechanism is operative for *Rb. sphaeroides* R-26.1, 2.4.1, and mutant GD(M203)/AW(M260) and indicates that A-branch charge separation proceeds at temperatures down to 10 K. The latter mechanism, derived from the spin polarization and operative for mutant LH(M214)/AW(M260), indicates that no long-lived radical pairs are formed upon direct excitation of the primary donor and that virtually no charge separation at the B-branch occurs at low temperatures. When the temperature is raised above 30 K, B-branch charge separation is observed, which is at most 1% of A-branch charge separation. B-branch radical pair formation can be induced at 10 K with low yield by *direct* excitation of the bacteriopheophytin of the B-branch at 590 nm. The formation of a carotenoid triplet state is observed. The rate of formation depends on the orientation of the reaction center in the magnetic field and is caused by a magnetic field dependence of the oscillation frequency by which the singlet and triplet radical pair precursor states interchange. Combination of these findings with literature data provides strong evidence that the thermally activated transfer step on the B-branch occurs between the primary donor, P_{865}, and the accessory bacteriochlorophyll, whereas this step is barrierless down to 10 K along the A-branch.

Photosynthesis is of vital importance for life on earth. In photosynthesis, large protein−cofactor complexes function as light-driven switches. These complexes catalyze a light-induced electron and proton transport across the photosynthetic membrane and have been optimized by nature to perform this task with a quantum efficiency close to unity. The prototype bacterial reaction centers (bRCs)[1] have been studied by many groups, and significant progress in the knowledge of the structure and function of the bRCs has been achieved (*1*−*8*). The first crystal structure of a bRC was determined in the 1980s (*3*, *9*−*11*). The prototypical reaction center from *Rhodobacter sphaeroides* is composed of three protein subunits, L, M, and H, with a molecular weight of 31, 34, and 28 kDa (*12*). The reaction center contains as cofactors four bacteriochlorophyll molecules (B, BChl), two bacteriopheophytins (H, BPheo), two ubiquinones, one carotenoid (spheroidene), and one non-heme iron (*3*). Two bacteriochlorophylls form a dimer, or special pair, called P_{865}, where the subscript denotes the wavelength of maximum absorption in the UV−vis spectrum. The other cofactors are arranged in two branches, denoted A-branch and B-branch, that show a pseudo-C_2 symmetry (see Figure 1).

Upon absorption of a photon from (sun)light at about 865 nm, an electron is excited at P_{865}. The exited electron subsequently travels to the final electron acceptor, the quinone on the B-branch (Q_B), by passing through a series of intermediate states. In the final charge-separated state, P_{865} is oxidized and Q_B is reduced. Earlier results derived mostly from optical spectroscopy of the native system showed that only the A-branch is active in charge separation with an efficiency of close to 1 (*5*, *13*, *14*) and that in the intermediate states the excited electron resides on one of the cofactors of the A-branch. After reaching Q_A, the electron then travels to the final acceptor, Q_B. Electron transfer along the B-branch

† This project was supported by the DFG-NWO International Collaborative Research Grant, project GA1100/1-2, and by the Research Grants NIH GM 41637 and DFG (SFB 663, TP A7).

* Author to whom correspondence should be addressed. Phone: ++49 208 306 3555. Fax: ++49 208 306 3951. E-mail vgastel@mpi-muelheim.mpg.de.

‡ Max-Planck-Institut für Bioanorganische Chemie.

§ University of California, San Diego.

[1] Abbreviations: B, bacteriochlorophyll; BChl*a*, bacteriochlorophyll *a*; BPheo, bacteriopheophytin; bRC, bacterial reaction center; Car, carotenoid; DAF, delay after flash; EPR, electron paramagnetic resonance; ESEEM, electron spin−echo envelope modulation; H, bacteriopheophytin; HOMO, highest occupied molecular orbital; isc, intersystem crossing; LUMO, lowest unoccupied molecular orbital; P_{865}, primary donor; *Rb.*, *Rhodobacter*; RP, radical pair; SO, spin orbit; SS, spin−spin; UQ, ubiquinone; ZFS, zero-field splitting.

10.1021/bi701593r CCC: $37.00
Published on Web 12/04/2007

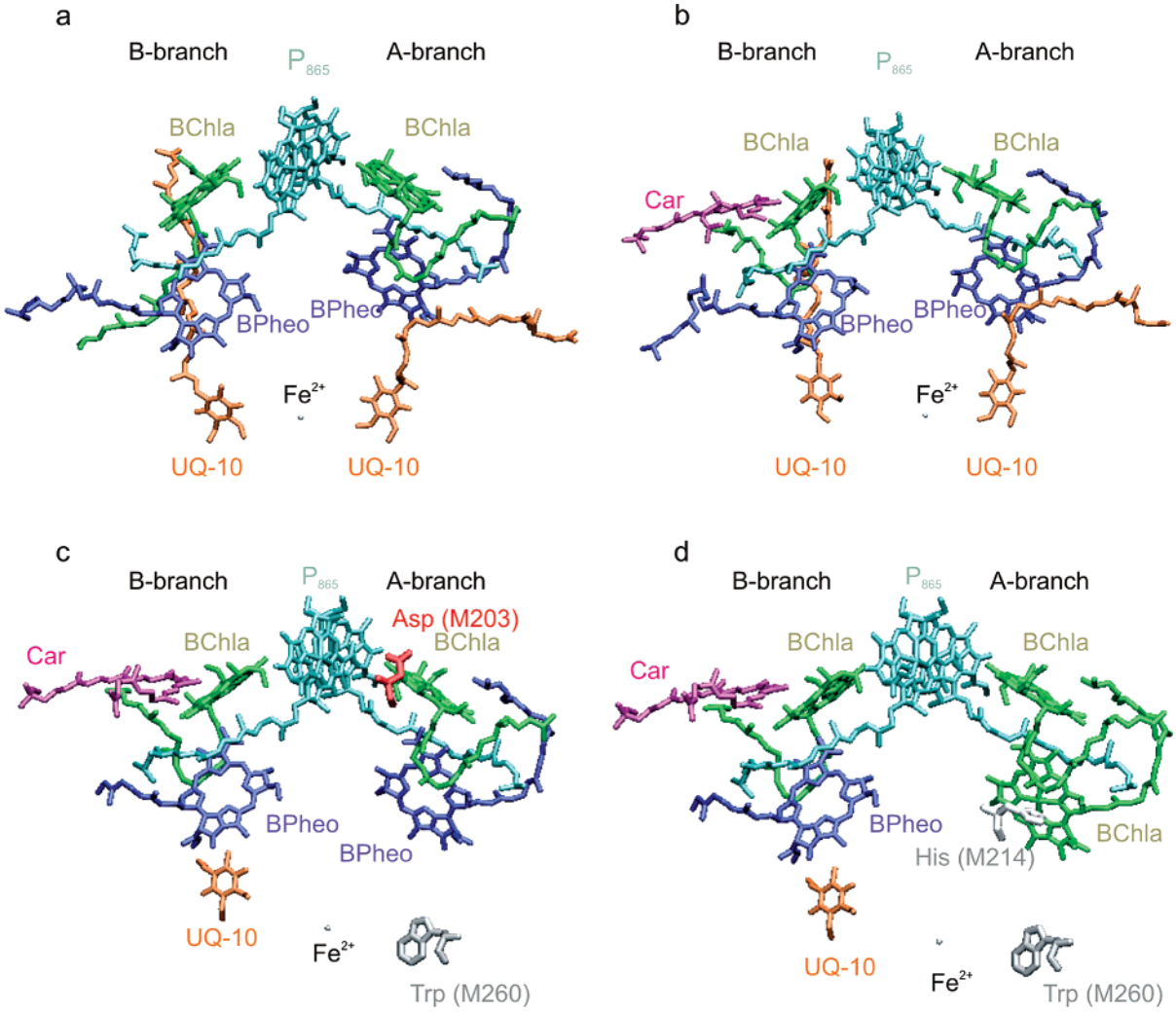

FIGURE 1: Cofactor arrangement in the bacterial reaction centers of (a) *Rb. sphaeroides* R-26.1 (PDB code: 1pcr), (b) *Rb. sphaeroides* 2.4.1 (PDB code: 4rcr), (c) *Rb. sphaeroides* double-mutant GD(M203)/AW(M260), and (d) *Rb. sphaeroides* double-mutant LH(M214)/AW(M260). The mutants are modeled after the structure of a quintuple mutant that contains all these mutations (PDB code: 1yf6) (*15*).

is found to be below 1% (*5*, *15*, *16*). According to Feher et al. (*5*) this arises from the breaking of the twofold symmetry at several places in the structure of the reaction center. Furthermore, inherent asymmetries in the dimer structure exist. The distance of the special pair with B_A is smaller than with B_B, bacteriopheophytin H_A is closer to B_A than H_B to B_B, and the detailed binding of the cofactors to the protein backbone is different in the two branches. It has been recently proposed that protein dynamics control the kinetics of the initial steps in the charge separation process (*17*).

Differences between A-branch and B-branch charge separation have so far been studied by optical spectroscopy (*18*−*20*). Upon excitation at 390 nm of *Rb. sphaeroides* reaction centers, a radical pair B^+H^- is formed on the B-branch that decays in picoseconds (*21*). This radical pair state has also been observed in mutated reaction centers upon excitation of the singlet excited states at different wavelengths (*21*), and B-branch electron transfer becomes possible by excitation to higher excited states of the reaction center (*22*). The largest B-branch radical pair formation in *Rb. sphaeroides* with efficiency of 35−45% has been found for a quadruple mutant in which a BPheo is introduced in place of B_B and a BChl*a* in place of H_A (*23*). In a *Rb. capsulatus* mutant the presently largest B-branch charge separation of 70% has been reported (*24*).

In this study, the triplet states of bacterial reaction centers and mutants thereof are investigated by EPR spectroscopy, to better understand the charge separation process and the directionality of charge separation with respect to the A- and B-branches. The triplet state is well suited for this, because the polarization pattern of the triplet state is determined by the precursor states directly after light excitation (*25*). Thus, by measuring the polarization pattern, information is obtained about whether or not the triplet state is derived from a long-lived radical pair state on either branch or whether other triplet-forming mechanisms are operative. Moreover, the rates of formation and decay of the paramagnetic species can be studied on a time scale of nanoseconds or longer. A disadvantage of the EPR technique is that singlet states cannot be detected. Therefore, the initial charge separation process, in which singlet radical pair states are involved, cannot be addressed directly by this method. Nevertheless, the EPR spectrum contains information about paramagnetic intermediates complementary to spectra obtained by fast optical techniques. In this respect, EPR spectroscopy can be used parallel with

Scheme 1

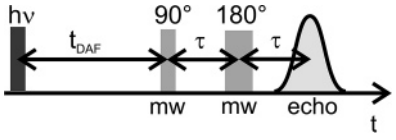

optical methods for the study of charge separation along the two branches.

In native reaction centers, the formation of the triplet state cannot compete with forward electron transfer. However, when the quinone acceptors are prereduced, an EPR spectrum of P_{865} in the triplet state ($^3P_{865}$) with a characteristic AEEAAE (A, absorptive; E, emissive) polarization is observed, which derives from a $P_{865}{}^+H_A{}^-$ radical pair (*2*). In case of different radical pair precursors, or other triplet-forming mechanisms, the polarization pattern of the observed $^3P_{865}$ triplet state is expected to be different. In our study we investigated triplet states of bacterial reaction centers for four species at Q-band microwave frequencies: first, *Rb. sphaeroides* R-26.1, which lacks the carotenoid spheroidene (Figure 1a). The second species is *Rb. sphaeroides* 2.4.1, used as a reference (Figure 1b). The third is the *Rb. sphaeroides* double-mutant GD(M203)/AW(M260), where the first mutation changes the H-bonding network near the accessory bacteriochlorophyll and makes the electron transport over the A-branch energetically less favorable (Figure 1c). The second mutation introduces a tryptophan in the binding pocket for Q_A, which blocks the access for the quinone at this position (*15*, *26*). The fourth species is the double-mutant *Rb. sphaeroides* LH(M214)/AW(M260), which introduces a histidine near the BPheo in the A-branch (Figure 1d), whereby a magnesium is incorporated into the BPheo which thus converts to BChl*a*.

The LH(M214) mutation has been extensively studied by Kirmaier, Holten and co-workers using fast optical techniques (*18*−*20*). The introduction of BChl*a* in the A-branch, also denoted as "β mutant" in literature, yields a short-lived radical pair state $P_{865}^{\bullet+}\,I^{\bullet-}$ upon excitation, where $I^{\bullet-}$ is most likely a BChl*a* species (*18*). Depending on the presence of additional mutations or the temperature, the lifetime of this radical pair state is $\leq$1 ns (*19*). The main effect of the LH(M214) mutation seems to be an increased charge recombination rate by a factor of about 20, which reduces the amount of $P_{865}^{\bullet+}\,Q_A^{\bullet-}$ to 60% as compared to 100% in native reaction centers.

For carotenoidless reaction centers of *Rb. sphaeroides* R-26.1 the triplet state $^3P_{865}$ was studied; for the other three systems the triplet states of $^3P_{865}$ *and* ^{3}Car. Carotenoids protect the photosynthetic apparatus from photoinduced damage by either trapping chlorophyll triplet states or quenching the excited singlet state of molecular oxygen (*27*). Spectroscopic and kinetic parameters are already available for carotenoids in bacterial reaction centers from earlier studies (*28*−*30*).

A requirement for a detectable EPR signal from $^3P_{865}$ that derives from a radical pair precursor is that the radical pair lives long enough to change from the singlet to the triplet state. A typical lifetime required for this process is 15 ns (*31*). Shorter lived radical pair states, e.g., as observed for LH(M214) mutants (*19*), remain in the singlet state and decay too fast to produce EPR-detectable signals. The presence of short-lived singlet radical pairs, can therefore not be detected by EPR spectroscopy and can thus at no stage be excluded from EPR measurements. In this study it is found that two triplet-forming mechanisms are operative and that charge separation along the A- and B-branches can be strongly influenced by mutations of amino acids near either of the branches.

MATERIALS AND METHODS

Experimental Details. Rb. sphaeroides R-26.1 was isolated and purified as described by Feher and Okamura (*32*) and those from *Rb. sphaeroides* 2.4.1 as described by Frank et al. (*33*). The quinones Q_A and Q_B were reduced as described in ref *34* by addition of sodium dithionite solution (0.5 M in 1 M Tris−HCl, pH 8.0) to yield a final dithionite concentration of 50 mM in the sample. *Rb. sphaeroides* mutants GD(M203)/AW(M260) and LH(M214)/AW(M260) were expressed and purified according to Paddock et al. (*15*). The mutants were not reduced with dithionite. Test measurements on mutants in which the quinones were reduced with dithionite gave the same results as those without dithionite reduction. The samples were frozen in liquid nitrogen in the dark. The quality of the samples was checked by UV−vis, SDS−PAGE, and special TRIPLE EPR (*35*, *36*) measurements at room temperature.

Electron spin−echo (ESE) detected and transient EPR spectra were recorded on a Bruker Q-band Elexsys E580 FT pulse EPR spectrometer equipped with a home-built EPR/ENDOR resonator (*37*) and an Oxford CF935 helium gas-flow cryostat for temperature control. Samples were excited with an Opotek OPO laser at variable wavelength, pumped by a Vibrant Nd:YAG laser at 10 Hz repetition rate. Excitation at 865 nm was performed with 5 mJ/pulse, at 537 and 590 nm with 6 mJ/pulse. The EPR measurements were performed in the temperature range of 10−130 K. The microwave frequency was typically 33.9 GHz, with variations of 0.2 GHz, depending on the identity of the sample and the temperature.

The two-pulse EPR, delay-after-flash (DAF)-EPR, and two-pulse electron spin−echo envelope modulation (ESEEM) experiments (*38*) are shown in Scheme 1. It consists of a laser pulse followed by two microwave pulses and detection by a Hahn echo. In the ESE-detected EPR experiments the magnetic field is swept, in DAF-EPR the magnetic field is fixed and the time t_{DAF} is swept, in two-pulse ESEEM, the time τ is swept. The length of the $\pi/2$ pulse was 40 ns, that of the π pulse was 80 ns. The delay between the two pulses was 440 ns, and the microwave power was 20 mW. The value for the delay was the minimum possible, taking into account the spectrometer dead time of about 400 ns. Some triplet EPR spectra recorded at larger delays times can be found in the Supporting Information. The accumulation time was typically 30 min for an EPR spectrum, except for mutant LH(M214)/AW(M260), which gave rise to much weaker signals. For this mutant the signal was accumulated for 8−12 h. With two-pulse EPR spectroscopy, the polarization pattern of the triplet state was measured, DAF-EPR was used to obtain information about kinetic parameters, like growth and decay rates of EPR signals, and with ESEEM spectroscopy, the hyperfine and quadrupole interaction of the pyrrole nitrogens can be investigated.

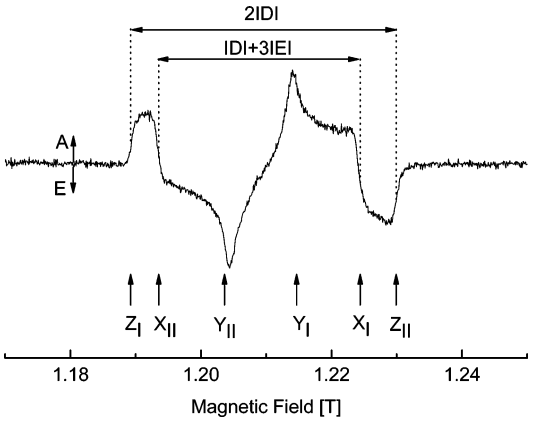

FIGURE 2: Q-band transient EPR spectrum of the bRC of *Rb. sphaeroides* R-26.1 at $T = 10$ K.

Transient EPR measurements were performed on the same spectrometer by using the Bruker "Specjet" oscilloscope as a transient recorder. The microwave power was 40 μW. The spectrum was accumulated with 200 averages. A spectrum took about 7 h of measurement time. Simulations of the triplet EPR spectra were performed with a self-written program based on the formalism described in ref *39*. For a more detailed description see the Supporting Information.

RESULTS

The Q-band transient EPR spectrum of *Rb. sphaeroides* R-26.1 is shown in Figure 2. The spectrum is comprised of absorptive (A) and emissive (E) signals. The width of the spectrum is determined by the zero-field splitting (ZFS) parameters *D* and *E*, and the observed polarization pattern AEEAAE is consistent with that reported earlier (*2*). The three canonical orientations, for which a molecule is oriented either with its *X*, *Y*, or *Z* axis of the ZFS tensor parallel to the magnetic field direction are indicated in the figure. They will be used as labels in the text. ESE-detected EPR spectra of *Rb. sphaeroides* R-26.1, 2.4.1, mutants GD(M203)/AW(M260) and LH(M214)/AW(M260), and BChl*a* in pyridine recorded at $T = 10$ K and $T = 50$ K are shown in Figure 3. The spectra at $T = 10$ K of *Rb. sphaeroides* R-26.1, 2.4.1 and GD(M203)/AW(M260) are similar. Strikingly, the EPR spectrum of *Rb. sphaeroides* LH(M214)/AW(M260) is completely different, and more similar to that of BChl*a* in pyridine. At $T = 50$ K, the polarization patterns of all spectra are different.

In the subsequent paragraphs, the EPR spectra, the polarization (A/E) patterns and the time and temperature dependences are described for each species.

Rb. sphaeroides R-26.1. The ESE-detected EPR spectrum of $^3P_{865}$ in *Rb. sphaeroides* R-26.1 at $T = 10$ K excited with a wavelength of 865 nm is characterized by the well-known polarization pattern AEEAAE (*2*). A narrow signal, marked with an asterisk, is present in the center of the spectrum, which belongs to a radical. A striking feature of the spectrum is that the emissive signals are systematically more intense than the corresponding absorptive signals, which contrasts with earlier measurements carried out at X-band frequencies using cw EPR (*2*) or transient EPR techniques. This is caused by a strong ESEEM effect at Q-band for the pyrrole nitrogens detected dominantly on the $M_S = 0 \leftrightarrow +1$ transition (vide infra).

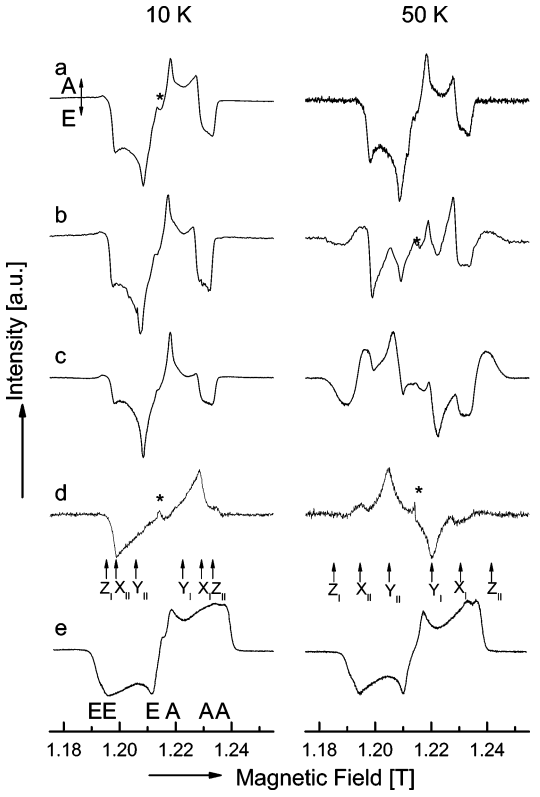

FIGURE 3: Q-band ESE-detected triplet EPR spectra in bRCs in *Rb. sphaeroides* at $T = 10$ K (left) and $T = 50$ K (right): (a) *Rb. sphaeroides* R-26.1, (b) *Rb. sphaeroides* 2.4.1, (c) *Rb. sphaeroides* GD(M203)/AW(M260), (d) *Rb. sphaeroides* LH(M214)/AW(M260), (e) ^{3}BChl*a* in pyridine. The signal marked with $*$ is assigned to a radical signal. The microwave frequency was typically 33.9 GHz with a variation of 0.2 GHz depending on the sample.

Table 1: ZFS Parameters for $^3P_{865}$ and ^{3}Car in *Rb. sphaeroides* R-26.1 and LH(M214)/AW(M260)[a]

	R-26.1		LH(M214)/AW(M260)	
	$^3P_{865}$	^{3}Car	$^3P_{865}$	^{3}Car
D [cm^{-1}]	0.0188	−0.0280	0.0188	−0.0280
E [cm^{-1}]	0.0031	0.0040	0.0039	0.0040
p_x			0.7	0.7
p_y			0.3	0.3
p_z			0.0	0.0
g_x	2.0033	2.0023	2.0033	2.0023
g_y	2.0038	2.0023	2.0042	2.0023
g_z	2.0023	2.0023	2.0023	2.0023
line width [mT]	0.8	0.8	0.8	1.0

[a] Those for *Rb. sphaeroides* 2.4.1 and the double-mutant GD(M203)/AW(M260) are the same within the error limits as those of R-26.1. Triplet decay rates are temperature dependent and given in Figure 4c−f. The error margins are as follows: D and E [±0.0002 cm^{-1}], p_x, p_y, and p_z [±0.05] with the constraint that $p_x + p_y + p_z = 1$, g_x, g_y, and g_z [±0.0003], line width [±0.2 mT].

The ZFS parameters *D* and *E* have been read from the spectrum and amount to $|D| = 0.0188$ cm^{-1}, $|E| = 0.0031$ cm^{-1}. They are given in Table 1 and agree well with those reported earlier (*2*, *34*). When the temperature is increased from 10 to 50 K, the shape of the EPR spectrum remains virtually the same and the amplitude decreases. The observation that the *D* and *E* parameters do not change indicates that the triplet state remains localized at $^3P_{865}$.

Information about the decay of the triplet sublevels of $^3P_{865}$ can be obtained by DAF-EPR measurements. In this experiment, EPR spectra are recorded as a function of the time

between the laser flash and the Hahn echo. The two-dimensional spectrum at $T = 10$ K is given as Supporting Information and is characterized by a slow decay with a time constant of 250 μs at the low- and high-field edges of the spectrum (B || Z_I and B || Z_{II}) and faster decays with time constants of both 80 μs for B || X_I, Y_I and B || X_{II}, Y_{II}. At both 10 and 50 K the decay behavior was found to be adequately described by a set of three time constants as given in formula (S3).

Rb. sphaeroides 2.4.1. The ESE-detected EPR spectrum of $^3P_{865}$ in *Rb. sphaeroides* 2.4.1, recorded at $T = 10$ K, is shown in Figure 3b. The spectrum is essentially the same as that recorded at 10 K for *Rb. sphaeroides* R-26.1. However, the EPR spectrum changes drastically when the temperature is increased to 50 K. Such a change in polarization pattern has been observed earlier (*28*, *29*) and was attributed to a triplet transfer to the carotenoid−spheroidene (*12*, *40*), hereafter referred to as carotenoid. At temperatures above 30 K, the polarization pattern changes significantly, which indicates a temperature-activated triplet transfer. The carotenoid triplet spectrum is broader and is characterized by different *D* and *E* parameters than that of $^3P_{865}$ (see Table 1). The EPR spectrum of the carotenoid is highly symmetric with respect to the relative intensity of the absorptive and emissive signals in the polarization patterns, and no ESEEM effects are observed. The carotenoid signal has a polarization pattern EAAEEA.

The triplet transfer from P_{865} to Car and the time evolution of both triplet signals has been measured by DAF-EPR at $T = 50$ K and is shown in Figure 4a. The $^3P_{865}$ signal is quenched quickly and anisotropically by the carotenoid with time constants of about 1 μs (B || Y, Z) and 4 μs (B || X), and the ^{3}Car signal decays to the ground state with time constants of 6 μs (B || Y, Z) and 14 μs (B || X). Two time traces recorded with B || X_{II} and B || Z_I are given in Figure 4b. A small fraction of the $^3P_{865}$ signal is not taken over by carotenoid, and the $^3P_{865}$ polarization can still be recognized at 8 μs after the laser flash. This residual $^3P_{865}$ signal decays to the ground state with a time constant of about 40 μs.

The temperature dependence of the time constants for formation and decay of the ^{3}Car signal is given in Figure 4, parts c and d. All time constants decrease with temperature. The time constant for B || X is about a factor of 3 larger than the time constants for B || Y, Z for both the formation and decay of the ^{3}Car signal.

Rb. sphaeroides GD(M203)/AW(M260). The third system under investigation is the *Rb. sphaeroides* double-mutant GD(M203)/AW(M260) (*15*). The EPR spectra at $T = 10$ K and $T = 50$ K are shown in Figure 3c. The spectrum at $T = 10$ K again looks similar to those of *Rb. sphaeroides* R-26.1 and *Rb. sphaeroides* 2.4.1 with minor changes, e.g., the intensities of the X_I and X_{II} transitions decrease so that the intensity of X_I becomes almost zero. This shows that also in this mutant the triplet state remains at $^3P_{865}$ at $T = 10$ K. At $T = 50$ K, the spectrum changes and the P_{865} triplet is again transferred to Car. By comparison with the spectrum of *Rb. sphaeroides* 2.4.1, it is seen that more ^{3}Car is present for mutant GD(M203)/AW(M260). In this mutant the triplet state is taken over faster by Car than in *Rb. sphaeroides* 2.4.1, and the signal is so large that it is possible to observe ^{3}Car signals with pulsed EPR methodology in our spectrometer up to 130 K. Above 130 K the relaxation processes reduce

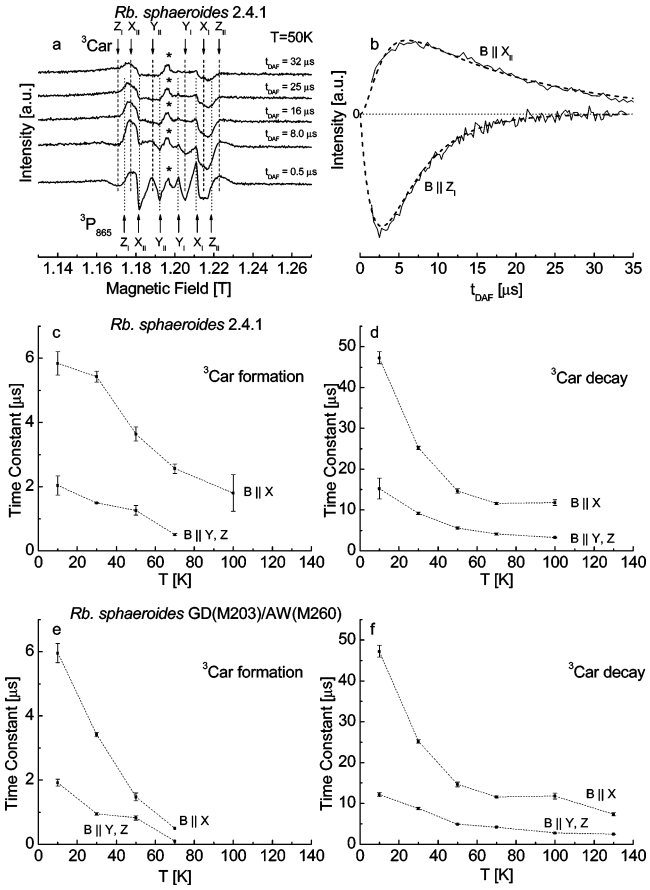

FIGURE 4: (a) ESE-detected EPR spectra of the $^3P_{865}$ and ^{3}Car triplet signals in *Rb. sphaeroides* 2.4.1 at 50 K recorded at different times after the laser flash. Dotted lines indicate the canonical orientations of $^3P_{865}$, dashed lines those of ^{3}Car. (b) Time traces of the EPR signal recorded at B || X_{II} and B || Z_I and simulations (dashed lines) using the model described in the Supporting Information. (c and d) Temperature dependence of time constants for ^{3}Car formation and decay in *Rb. sphaeroides* 2.4.1. (e and f) Temperature dependence of time constants for ^{3}Car formation and decay in *Rb. sphaeroides* GD(M203)/AW(M260).

the signal below the noise level, hampering detection. The temperature dependence of the decay and growth constants is shown in Figure 4, parts e and f. The growth constant for B || X decreases faster with higher temperatures in mutant GD(M203)/AW(M260) than in *Rb. sphaeroides* 2.4.1 (Figure 4d). The time constants for the decay of the ^{3}Car signal have the same temperature dependence in *Rb. sphaeroides* 2.4.1 and mutant GD(M203)/AW(M260).

In Figure 5, two-pulse ESEEM spectra and modulation patterns recorded at B || Z_I and B || Z_{II} are depicted. At these field positions, the same set of molecules is selected—those that are oriented with the principal *Z* axis of the ZFS tensor parallel to the magnetic field. At the latter magnetic field setting, only shallow modulations are observed, whereas at B || Z_I, deep modulations are visible, explaining the observed asymmetry of the Q-band ESE-detected EPR spectra. The modulations are caused by the presence of nuclei with $I > 0$, in this case the four pyrrole nitrogens ($I(^{14}N) = 1$), whose hyperfine interaction is of the same order as the nuclear Zeeman interaction, which is known as the "exact cancellation" condition (*41*). Large modulations are observed when the exact cancellation condition is fulfilled (*41*). In this case it is fulfilled better at B || Z_I than B || Z_{II}, and the implications will be discussed further in the discussion.

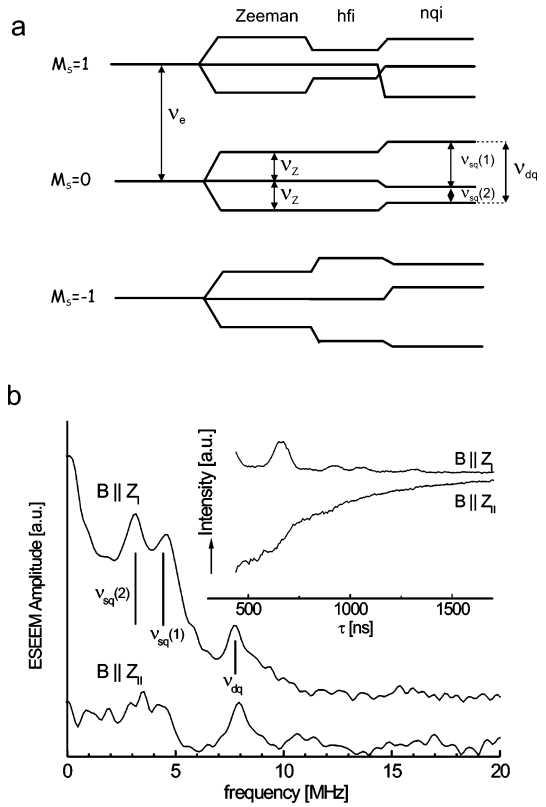

FIGURE 5: (a) Schematic energy level diagram for a nuclear spin $I = 1$ and electron spin $S = 1$ in a magnetic field, including nuclear Zeeman, hyperfine (hfi), and nuclear quadrupole (nqi) interactions. The three frequencies $\nu_{sq}(1)$, $\nu_{sq}(2)$, and ν_{dq} of the $M_S = 0$ manifold dominate the ESEEM spectrum. (b) Two-pulse ESEEM spectra and modulation patterns (inset) of $^3P_{865}$ recorded for *Rb. sphaeroides* GD(M203)/AW(M260) at the Z_I (low-field) and Z_{II} (high-field) canonical orientations (see Figure 2). The modulation depth at Z_I is about 4 times larger than at Z_{II}. The temperature is 10 K, and no contribution of carotenoid was detected in the EPR spectrum.

The frequencies at 3.2, 4.6, and 7.8 MHz are observed in both ESEEM spectra with only a small difference of ±0.2 MHz. Also, the latter frequency is the sum of the former two frequencies, which shows that 7.8 MHz concerns the double-quantum transition and that all frequencies stem from the $M_S = 0$ manifold (see Figure 5a). Taking advantage of the fact that no hyperfine interaction is present in the $M_S = 0$ level, an estimate of the size of the quadrupole interaction for the pyrrole nitrogens can be made by using the formula (*38*)

$$\nu_{dq} = 2\sqrt{\nu_Z^2 + \frac{e^2qQ}{4h}(3+\eta^2)} \qquad (1)$$

where ν_Z is the Zeeman frequency for ^{14}N and e^2qQ/h and η are the nuclear quadrupole coupling parameters (*42*). The asymmetry parameter η is defined as

$$\eta = \frac{Q_{xx} - Q_{yy}}{Q_{zz}} \qquad (2)$$

where Q_{xx}, Q_{yy}, and Q_{zz} are electric field gradients at the nitrogen. The asymmetry parameter ranges between 0 and 1, and its exact value only influences that of e^2qQ/h by about 0.4 MHz. By using eq 1, a value of $e^2qQ/h = 3.2 \pm 0.3$ MHz is found.

Rb. sphaeroides LH(M214)/AW(M260). Figure 3d shows the ESE-detected EPR spectrum of $^3P_{865}$ in *Rb. sphaeroides* LH(M214)/AW(M260) in frozen solution. The spectrum has a polarization pattern EEEAAA, which is completely different from those of the triplet spectra of $^3P_{865}$ in *Rb. sphaeroides* R-26.1, 2.4.1, and GD(M203)/AW(M260). The signal in mutant LH(M214)/AW(M260) is weaker by a factor of about 300 in comparison to the triplet signals in the other three systems; nevertheless, the *D* value for mutant LH(M214)/AW(M260) remains the same and the *E* value (0.0039 cm^{-1}) is only slightly increased. Therefore, this triplet state is most likely also stems from P_{865}. The EEEAAA polarization pattern in this mutant is similar to that of a BChl*a* monomer in vitro, shown in Figure 3e, which is formed by an intersystem crossing rather than a radical pair mechanism. The signal at Z_I is further attenuated by the ESEEM effect and can barely be seen.

At $T = 50$ K, the EPR signal changes as compared to $T = 10$ K. The polarization pattern becomes EAAEEA, and the Z_I and Z_{II} transitions are very weak. Strikingly, the *D* and *E* parameters read from the spectrum at $T = 50$ K agree with those of ^{3}Car observed in the other three systems, but again the polarization pattern is different. Almost no contribution of $^3P_{865}$ signal is observed in the spectrum at $T = 50$ K anymore, which indicates that the time constants for quenching of $^3P_{865}$ by the carotenoid are even shorter here than in mutant GD(M203)/AW(M260), but the temperature threshold remains about 30 K.

Additional EPR experiments have been performed with excitation wavelength $\lambda = 537$ nm and $\lambda = 590$ nm. The motivation for these experiments is that at 537 nm the remaining BPheo in the B-branch is excited and at 590 nm all BChl*a* molecules are excited. At the former wavelength B-branch charge separation can therefore be selectively studied. In both cases, the absolute signal is decreased as compared to excitation at 865 nm, indicating less efficient triplet formation. The spectra at $T = 10$ K are shown in Figure 6. Excitation at 537 nm introduces small but important changes in the polarization pattern, marked with arrows in Figure 6b, whereas excitation at 590 nm does not alter the spectrum as compared to excitation at 865 nm. The changes occur exactly at the Y_I and Y_{II} canonical orientations of $^3P_{865}$ and show an emissive signal at low field and an absorptive signal at high field. The polarization of these additional signals is the same as that of the Y_I and Y_{II} orientations for *Rb. sphaeroides* R-26.1, 2.4.1, and GD(M203)/AW(M260).

Simulations. Simulations of the EPR spectra for all four systems are shown in Figure 7. They are simulated by either a radical pair or intersystem crossing mechanism and concern simulations for $^3P_{865}$ (left column) and ^{3}Car (right column). The simulations reproduce the positions of essentially all bands in the spectra and the overall line shape. Some mismatches with respect to the line shape occur because of the presence of a large ESEEM effect in the pulsed EPR spectra at Q-band (vide infra); for example, at the low-field side in Figure 7b, the simulation shows an emissive feature that is suppressed in the experimental spectrum by the ESEEM effect. The parameters used in the simulation are shown in Table 1. The ZFS parameters *D* and *E* for $^3P_{865}$ are essentially the same in all four systems under investigation, as are those for ^{3}Car. Also, for $^3P_{865}$ the effect of anisotropy of the **g** tensor ($g_x \neq g_y \neq g_z$) can be observed in

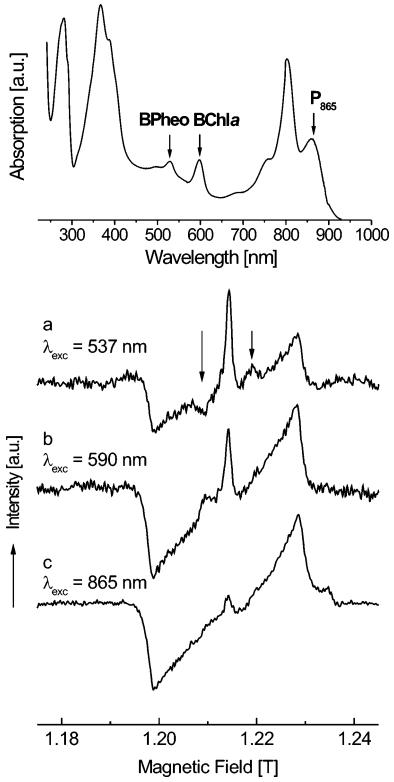

FIGURE 6: (Top) UV−vis spectrum and ESE-detected EPR spectra of $^3P_{865}$ in *Rb. sphaeroides* LH(M214)/AW(M260) at $T = 10$ K. (Bottom) EPR spectra recorded with laser excitation of wavelength (a) 537, (b) 590, and (c) 865 nm. The labels in the UV−vis spectrum indicate absorbing cofactors. The arrows at the spectrum with (a) $\lambda_{exc} = 537$ nm and $T = 10$ K indicate additional signals of low intensity which correspond to the RP triplet state of $^3P_{865}$.

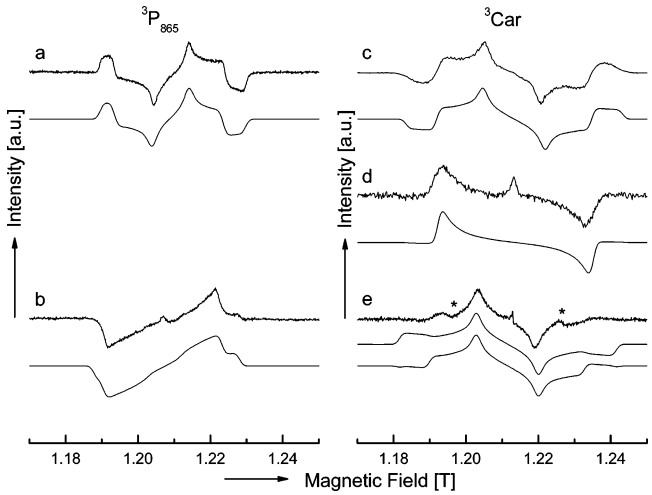

FIGURE 7: EPR spectra (upper trace) and simulations (lower traces) of the $^3P_{865}$ and ^{3}Car triplet states in bacterial reaction centers of *Rb. sphaeroides*: (a) transient EPR, $^3P_{865}$ in *Rb sphaeroides* R-26.1, $T = 10$ K; (b) ESE-detected EPR, $^3P_{865}$ in *Rb. sphaeroides* LH(M214)/AW(M260), $T = 10$ K, $t_{DAF} = 500$ ns; (c) ESE-detected EPR, ^{3}Car in *Rb. sphaeroides* GD(M203)/AW(M260), $T = 70$ K, $t_{DAF} = 500$ ns; (d) ESE-detected EPR, ^{3}Car in *Rb. sphaeroides* GD(M203)/AW(M260), $T = 70$ K, $t_{DAF} = 25$ μs; (e) ESE-detected EPR, ^{3}Car in *Rb. sphaeroides* LH(M214)/AW(M260), $T = 50$ K, $t_{DAF} = 500$ ns. The signals marked with $*$ belong to a small contribution of $^3P_{865}$, which has not yet fully decayed. The middle trace in (e) is a simulation assuming a pure isc mechanism; in the lower trace 50% isc and 50% RP mechanism efficiency was used.

the EPR spectrum. For example, the width of the low-field signal in the EPR spectrum of $^3P_{865}$ is smaller than that of the high-field signal. This effect can only be simulated by inclusion of an anisotropic **g** tensor. In the EPR spectra for ^{3}Car, the signals at low field and high field have the same width, and no **g** tensor anisotropy can be observed.

DISCUSSION

The Q-band ESE-detected EPR spectra of *Rb. sphaeroides* R-26.1, 2.4.1, and the mutants GD(M203)/AW(M260) and LH(M214)/AW(M260) shown in Figure 3 display different polarization patterns and temperature behavior. Though some of these observations are already known from earlier studies at different microwave frequencies, several new observations related to A- and B-branch charge separation are made here. In the discussion, these new observations are interpreted and discussed, and a comparison is made with existing literature data where possible. First, the polarization patterns of the EPR spectra are discussed. They are related to the mechanism by which the triplet state of $^3P_{865}$ is formed and thereby give information about radical pair precursor states on either the A- or B-branch and the charge separation processes of both branches. Second, the dynamics and temperature dependence of triplet−triplet energy transfer from $^3P_{865}$ to ^{3}Car is discussed. An interesting observation here is that the triplet−triplet transfer is found to be anisotropic; it depends on the orientation of the bRC in the magnetic field. Last, the additional signals in mutant LH(M214)/AW(M260) upon excitation at 537 nm are discussed. This mutant has only one remaining bacteriopheophytin in the B-branch, and B-branch charge separation can thus be selectively investigated by excitation at 537 nm.

Polarization Pattern, Intersystem Crossing, and Radical Pair Mechanisms. In *Rb. sphaeroides* 2.4.1, R-26.1, and mutant GD(M203)/AW(M260), the triplet state is formed after light excitation by a radical pair mechanism (Figure 8a). In this mechanism, the excited electron is transferred from P_{865} to bacteriopheophytin (H) on the A-branch and forms a radical pair $P_{865}^{\bullet+}$ $H_A^{\bullet-}$ (*2*, *4*, *6*, *13*). The radical pair state is initially present as a singlet state. However, since the unpaired electrons are located on different molecules, they feel a different effective magnetic field (*31*). Because the singlet state remains virtually degenerate with the T_0 sublevel of the triplet radical pair state, a significant mixing of the S and T_0 levels occurs, in which the radical pair states oscillate back and forth between S and T_0. The T_0 radical pair state can then recombine to form $^3P_{865}$. This mechanism is also called the S−T_0 mechanism (*33*). In the radical pair mechanism the $M_S = 0$ sublevel of $^3P_{865}$ is exclusively populated. This implies that shortly after the laser flash and before decay processes play a role, all $T_0 \rightarrow T_{+1}$ transitions are absorptive and $T_0 \rightarrow T_{-1}$ are emissive, as is explained in Figure 8a. A polarization pattern AEEAAE is observed, which means that the zero-field parameter D is positive, consistent with previous results (*2*, *4*, *6*, *34*). The quantum yield of $^3P_{865}$ formation in reduced reaction centers at temperatures below 50 K is found to be close to unity; at 300 K it is about 15% (*13*, *28*).

The triplet radical pair mechanism also implies that the amplitudes of the absorptive and emissive signals are identical. This is indeed observed in transient EPR spectra (see Figure 2 and ref *28*). However, the ESEEM effect (*38*, *43*−*46*) may introduce a modulation of the ESE amplitude

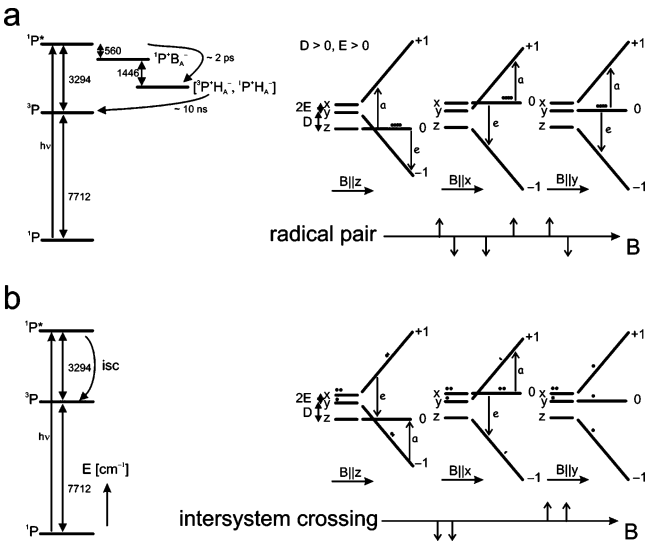

FIGURE 8: (a) Triplet formation in bacterial reaction centers of *Rb. sphaeroides* R-26.1, 2.4.1, and GD(M203)/AW(M260) by the radical pair mechanism. Energies are in wavenumbers and reproduced from refs *5* and *13*. Also indicated is the splitting for the triplet sublevels for the magnetic field direction parallel to the *X*, *Y*, or *Z* principal axis of the ZFS tensor. All population is located in the $M_S = 0$ sublevel; the resulting polarization pattern is of the ESE-detected EPR spectrum. (b) Triplet formation in the bacterial reaction center of *Rb. sphaeroides* LH(M214)/AW(M260) by the intersystem crossing (isc) mechanism. The splitting of the triplet sublevels is identical to (a), but the population is distributed as described by eq S1, resulting in a different polarization pattern. P: special pair (bacteriochlorophyll dimer), B_A: accessory bacteriochlorophyll, H_A: bacteriopheophytin (both in the A-branch).

in pulsed EPR spectroscopy. For nuclei with $I > 0$, in this case the four pyrrole nitrogens, whose hyperfine interaction is of the same order as the nuclear Zeeman interaction (*41*), deep modulations can be observed. This phenomenon is known as the "exact cancellation" condition (*41*) and essentially means that in one of the M_S manifolds, the nuclear Zeeman and hyperfine splitting virtually cancel each other and cause a large mixing of the nuclear spin sublevels. Though normally applied to doublet ($S = {}^1/_2$) states, the exact cancellation condition works similarly for triplet states. For triplet states, the $M_S = 0$ manifold is not split further by nuclear hyperfine interaction (see Figure 5a). Depending on the sign of the hyperfine interaction, cancellation occurs either in the $M_S = +1$ or $M_S = -1$ manifold. Therefore, out of the two possible EPR transitions ($M_S = 0 \leftrightarrow +1$ and $M_S = 0 \leftrightarrow -1$) the ESEEM effect will be large only for the EPR transition that involves the "cancelled" M_S level and small for the other EPR transition.

The behavior described in the previous paragraph is exactly what is observed in the two-pulse ESEEM experiments on $^3P_{865}$. A strong ^{14}N ($I = 1$) modulation for B || Z_I, which with positive *D* corresponds to the $M_S = 0 \leftrightarrow +1$ transition and a shallow modulation for B || Z_{II}, which is the $M_S = 0 \leftrightarrow -1$ transition. This allows the identification of the relative sign of the hyperfine interaction with respect to that of *D*. Since *D* is known to be positive (*4*, *6*), it means that the $M_S = +1$ manifold is cancelled and the sign of the hyperfine interaction of the pyrrole nitrogens must thus also be positive.

Another attractive feature unique to triplet states is that the ^{14}N quadrupole interaction can be directly determined from the frequencies of the $M_S = 0$ manifold. Since no hyperfine interaction is present in this M_S manifold, the nuclear frequencies are well separated from those of the cancelled $M_S = +1$ manifold. The latter are close to 0 MHz and give rise to the intense band close to 0 MHz in the ESEEM spectrum at B || Z_I (cf., Figure 5). The frequencies of the $M_S = 0$ manifold are expected around the ^{14}N Zeeman frequency (3.6 MHz at B || Z_I) and the double of this frequency. Under the assumption that the four pyrrole nitrogens have a very similar quadrupole splitting, the quadrupole parameter $e^2qQ/h = 3.2 \pm 0.3$ MHz has been read from the spectrum (cf., Results), which is of similar magnitude to that observed in experiments at X-band (3.76 MHz (*47*)). The discrepancy may stem from the fact that at X-band frequency the quadrupole splitting is large enough to cause significant mixing of the nuclear spin sublevels even without hyperfine interaction in the $M_S = 0$ manifold, and therefore, the X-band spectra are significantly more difficult to interpret.

A simulation based on the radical pair mechanism of a transient EPR spectrum recorded at $T = 10$ K shortly after the laser flash is shown in Figure 7a for *Rb. sphaeroides* R-26.1. In the transient EPR spectrum, no ESEEM effects are present and the spectrum displays absorptive and emissive signals of equal intensity. The spectrum is also representative for *Rb. sphaeroides* 2.4.1 and mutant GD(M203)/AW(M260) at $T = 10$ K. All features of the experimental spectrum are reproduced, and the simulation parameters are included in Table 1. The *D* parameter is 0.0188 cm^{-1}, identical to the one read directly from the spectrum. The different widths of the low-field and high-field signals are attributed to a small anisotropy of the **g** tensor of $^3P_{865}$ (*48*, *49*). In the simulation in ref *48*, the **g** tensor was assumed to be collinear with the ZFS tensor. We also use this approximation and the three *g* values amount to 2.0033, 2.0038, and 2.0023, respectively. These numbers are similar, but not identical to the ones found in measurements at 130 and 95 GHz (*48*, *49*), which are also not identical. The discrepancies, which stem from differences of only a few gauss, likely come from the contribution of ^{14}N hyperfine couplings to the width of the EPR spectrum, that become less important at high microwave frequencies.

The ESE-detected EPR spectrum of mutant LH(M214)/AW(M260) does not display a polarization pattern typical for a radical-pair-based triplet state. Rather the pattern is similar to that recorded for ^{3}BChl*a* in vitro (cf., Figure 3, parts d and e), which is formed by an intersystem crossing (isc) mechanism. In this mechanism, depicted in Figure 7b, the excited electron does not leave P_{865}. Spin-dependent processes, most notably spin−orbit (SO) coupling and spin−spin (SS) interaction (*50*), then flip the spin of one of the unpaired electrons to form $^3P_{865}$. This triplet state is identical to the one formed by the radical pair mechanism in the other three systems, but because of the different precursor state (i.e., P^*_{865}), the relative populations of the triplet sublevels and hence the polarization pattern differ completely. The populations for an isc triplet are given by formula (S*2*). By using this formula, the ESE-detected EPR spectrum at $T = 10$ K for mutant LH(M214)/AW(M260) can indeed be simulated by using virtually identical parameters used for the simulation—only g_y has changed to 2.0042—of the radical pair triplet, and a population distribution of the ZFS levels

p_x, p_y, and p_z of 0.7, 0.3, and 0.0, respectively. The only discrepancy concerns a difference in amplitude at the low-field side, which stems from the ESEEM effect that is not included in the simulation. The simulation is given in Figure 7b.

The observation of an isc triplet and not an RP triplet in mutant LH(M214)/AW(M260) has two important consequences for the charge separation process. First, the LH(M214) mutation completely inhibits long-lived radical pair formation at the A-branch. Second, also no long-lived radical pair is formed at $T = 10$ K in the B-branch. This is in line with the observations that the lifetime of a transient radical pair is so short (*19*) that the spin state remains a singlet (*31*). Since no mutation has been introduced at the B-branch in this mutant, the second observation is likely valid for all systems. In the wild type case, the A-branch electron transfer proceeds at temperatures down to 10 K, the B-branch transfer has a thermal activation barrier of 30 K (*51*).

Anisotropy of Triplet−Triplet Transfer Dynamics and Relaxation Processes. After formation of $^3P_{865}$, spin-dependent interactions convert the triplet state back into the ground state. The decay rates are in general temperature dependent. When a carotenoid is present, the triplet state is taken over by ^{3}Car from $^3P_{865}$ via a Dexter energy transfer mechanism, since ^{3}Car is lower in energy than $^3P_{865}$ (*30*, *51*−*53*). The energy transfer from P_{865} to Car occurs via the accessory BChl*a* in the B-branch, and the rate of the transfer is determined by the activation barrier between P_{865} and BChl*a* (*30*, *54*). The triplet state of the accessory BChl*a* in the B-branch of wild-type *Rb. sphaeroides* has never been observed, which indicates that the subsequent transfer to carotenoid is essentially activationless and very fast (*30*). If the carotenoid is not present, e.g., in *Rb. sphaeroides* R-26.1, $^3P_{865}$ decays back to the ground state, and also a monomeric bacteriochlorophyll triplet was observed by optically detected magnetic resonance (ODMR) experiments (*55*, *56*). In triplet−triplet transfer, as well as the decay of ^{3}Car to the ground state, again a spin crossover has to take place. The same interactions that are responsible for the formation of the isc triplet are also responsible for this spin crossover, and the decay rates k_i are described by eq S3.

For *Rb. sphaeroides* R-26.1 decay times of 80 μs were observed in the DAF-EPR measurements at $T = 10$ K for the X and Y transitions and 250 μs for the Z transition. These results agree with those from transient EPR spectroscopy on *Rb. sphaeroides* (*27*, *57*). Indeed, it is already known that the X and Y sublevels are mainly responsible for deactivation of the triplet state of chlorophylls and derivatives (*58*). Metz has shown that for planar aromatic systems one would expect that in calculating the spin vibronic coupling term, the spin sublevels corresponding to the in-plane molecular axes (*X* and *Y*) associated with a $\pi\pi^*$ triplet state derive their isc activity from first-order, one-center spin−orbit coupling with singlet $\sigma\pi^*$ and $n\pi^*$ levels, whereas the Z spin sublevel must utilize higher order one-center terms to gain appreciable activity (*59*); therefore the population and depopulation rates for the Z level will always be smaller than those for the X and Y levels (*27*, *28*, *58*).

For *Rb. sphaeroides* 2.4.1 and mutant GD(M203)/AW(M260) large changes in the triplet EPR spectra are observed upon increase of the temperature to 50 K (cf., Figure 3). The shape of the spectrum changes because above 30 K the triplet state is taken over by carotenoid (*28*). Monger et al. (*60*) concluded that the carotenoid triplet was formed by energy transfer from $^3P_{865}$. Since the energy transfer rate from the donor to the acceptor triplet occurs on a time scale which above 30 K becomes fast compared with spin−lattice relaxation, the acceptor triplet spectrum will also display a radical pair polarization pattern (*29*). The carotenoid triplet has a polarization pattern EAAEEA, which is opposite to the polarization pattern AEEAAE of $^3P_{865}$ (*28*). The difference can be explained where the *D* value of ^{3}Car is opposite to that of the donor ($^3P_{865}$), i.e., negative (*28*). In mutant GD(M203)/AW(M260), the pure ^{3}Car signal could be measured by pulsed EPR shortly after the laser flash before decay processes could take place. The simulation using a RP mechanism is shown in Figure 7c, the simulation parameters are given in Table 1. The DAF-EPR spectra of ^{3}Car at 70 K can be simulated satisfactorily with three time constants, $k_y = k_z = 4$ μs, $k_x = 13$ μs. As an example, the ^{3}Car signal at $t_{DAF} = 25$ μs is simulated in Figure 7d, where it is indeed seen that only intensity at the X orientations remains present. The temperature dependence of these numbers is given in Figure 4f. The same temperature dependence is found for *Rb. sphaeroides* 2.4.1 (Figure 4d), and the numbers agree with previous studies (*27*, *57*).

So far unreported observations concern the anisotropic triplet−triplet transfer described by three growth constants for the ^{3}Car signal and the process responsible for ^{3}Car formation in mutant LH(M214)/AW(M260). These will be discussed next.

Essentially over the temperature range from 10 to 70 K, the ^{3}Car signal does not grow isotropically for both *Rb. sphaeroides* 2.4.1 and mutant GD(M203)/AW(M260). At B || X, the rate constant for growth is a factor of 3 faster than at B || Y and B || Z (Figure 4). The initially puzzling result can be rationalized if all precursor states including the radical pair states are considered, and it also gives a clue as to why the ratio of three between the growth constants is remarkably constant over the examined temperature range: as reported by Frank and co-workers, the energy transfer from the donor to the acceptor triplet occurs on a fast time scale compared to spin−lattice relaxation (*30*, *51*). However, the oscillation frequency ν_{S-T_0} between the singlet and triplet radical pair states is on the order of 15 MHz (*61*), which is similar to the Dexter energy transfer rate. The frequency ν_{S-T_0} depends on the orientation of the molecule in the magnetic field, and since other rate constants are of similar magnitude, this dependence of ν_{S-T_0} is mirrored into the growth rates of the ^{3}Car signal.

An anisotropic, orientation-dependent quantum yield of $^3P_{865}$ has been reported at 130 GHz owing to this effect, which is expected to become negligible at lower microwave frequencies (*48*). Though anisotropy in quantum yield is indeed not observed at 34 GHz, the anisotropy of the dynamics and associated rate constants *are* detectable at Q-band microwave frequencies. The anisotropy of ω_{S-T_0} can be detected on the ^{3}Car signal if the other time constants, e.g., for radical pair recombination to $^3P_{865}$, are faster or of similar magnitude. Most likely, the anisotropy of ω_{S-T_0} is also visible in the growth constants of $^3P_{865}$; the latter could unfortunately not be detected due to the spectrometer dead time.

The growth curves for the ^{3}Car signal have been fitted using the model described in the Supporting Information, and fits are included in Figure 4b as an example. At $T = 50$ K, the experimentally observed formation behavior of the ^{3}Car signal in *Rb. sphaeroides* 2.4.1 can be understood by assuming that ω_{S-T_0} is equal to 100 MHz for B || Y, Z and 13 MHz for B || X (see the next paragraph). In the model, the time constant for radical pair recombination was taken to be 10 ns, the isotropic Dexter energy transfer constant 1.7 μs. Thus, the slow interconversion of the singlet and triplet radical pairs at B || X leads to a slower buildup of the ^{3}Car signal at B || X as compared to B || Y or Z, even when the Dexter energy transfer rate is isotropic, i.e., not dependent on the orientation of the bRC in the magnetic field.

The spread in ω_{S-T_0} of one order of magnitude used in the model is large. However, the frequency of the radical pair oscillation indeed seems to be very orientation dependent if measured on the triplet radical pair state directly. This is confirmed by transient EPR measurements reported in ref *61*, particularly in Figure 3, where a large variation of ω_{S-T_0} with selected orientation is observed. An alternative model that includes the possibility of carotenoid in two or even more conformations (*40*, *52*, *53*, *62*) was found insufficient to explain the observed anisotropy of the ^{3}Car growth constants, since the presence of multiple conformations would just lead to multiple, but isotropic growth constants (though the employed model does not rule out the presence of multiple conformations of the carotenoid). Also, a three-spin model described in literature (*31*), which includes a third electron spin on Q_A, has been tested but was found to be inadequate, since the mutant GD(M203)/AW(M260) effectively has no Q_A and still displays virtually identical behavior as *Rb. sphaeroides* 2.4.1. As noted in ref *48* the anisotropy of triplet formation introduced by that of ω_{S-T_0} depends strongly on the relative orientations of the **g** tensors of the radical pair constituents. An even more sophisticated model that explicitly includes these quantities and their relative orientations to the ZFS and **g** tensor of ^{3}Car would lead to too many parameters in the simulation and has therefore not been attempted.

Now the double-mutant LH(M214)/AW(M260) is considered, which displays a $^3P_{865}$ signal at $T = 10$ K formed by isc (Figure 8b). Since Dexter energy transfer is a spin-conserving process, the polarization pattern of $^3P_{865}$ is expected to be taken over by ^{3}Car under conservation of the spin polarization. This is indeed the case. At $T = 50$ K, the EPR spectrum can be simulated by using the *D* and *E* parameters for ^{3}Car and using the same population distribution that was required to simulate $^3P_{865}$ in this mutant. The simulation is shown in the center trace of Figure 7e, and the parameters are included in Table 1.

At the low-field (Z_I) and high-field (Z_{II}) edges, the simulation does not agree with the experimental spectrum, for which the signal is close to zero. It can be shown that if only the isc mechanism populates the triplet state, an intensity of zero along Z would mean equal intensities at the X and Y canonical orientations. This is not observed experimentally. Thus the experimental spectrum at $T = 50$ K cannot result solely from an isc mechanism. A more plausible explanation for the mismatch at the low-field and high-field sides is that at $T = 50$ K, also the RP mechanism becomes operative in populating the triplet state. For the RP mechanism the simulation is shown in Figure 7c. If 50% efficiency for both the isc and RP mechanisms is assumed, the experiment and simulation agree very well, as seen in Figure 7e. This has important consequences for the charge separation process, as the RP mechanism implies the formation of a radical pair species. Because mutant LH(M214)/AW(M260) does not have a BPheo in the A-branch owing to the LH(M214) mutation, the radical pair must have formed on the B-branch, and it seems that at temperatures of 50 K and above, the B-branch becomes active in radical pair formation. From the signal-to-noise ratio, the B-branch charge separation amounts to at most 1% as compared to A-branch charge separation in the native system, which is much more efficient (*15*, *16*, *63*, *64*).

Wavelength Dependence of $^3P_{865}$ Formation. In mutant LH(M214)/AW(M260), $^3P_{865}$ at $T = 10$ K is formed by an isc mechanism upon direct excitation at 865 nm. This mutant contains only one remaining BPheo in the B-branch. This system is therefore ideally suited to investigate the B-branch charge separation process since it allows a selected excitation of the BPheo at 537 nm, where no other pigments absorb. Upon excitation at 537 nm, the absolute signal becomes smaller and acquisition of the triplet ESE-detected EPR spectrum with a signal-to-noise ratio of about 5 requires averaging of close to 12 h. However, the shape of the EPR spectrum displays minor changes as compared to that with excitation at 865 nm.

The *D* and *E* parameters of the spectrum at 865 nm excitation are identical to the ones observed for $^3P_{865}$ in Figure 3a−d. Thus, the spectrum recorded after excitation at 537 nm is also assigned to $^3P_{865}$. A possibility that the spectrum contains part of a BPheo triplet is unlikely, since the spectrum does not agree with the ZFS parameters for BPheo in vitro. It is known that the BPheo isc triplet EPR spectrum has polarization E at Y_{II} and A at Y_I (*2*), instead of the A, E polarizations observed here. An A and E polarization seems to be quite unique to the RP mechanism for triplet formation, see Figure 3.

The question then is how does the triplet state end up at P_{865} after excitation of BPheo and by which mechanism are the two additional "RP-like" signals at the Y canonical orientations formed? Formally, these processes occur on a faster time scale than that of the EPR experiment; an answer fully substantiated by EPR spectroscopy can therefore not be given. The EPR spectra, however, indicate the following. Most likely, most of the excitation energy is transferred from H to P_{865}: $(P_{865}H^*) \rightarrow (P^*_{865}\,H)$, and then the isc triplet on P_{865} is formed. This would yield the same spectrum as that after excitation at 865 nm. Additionally, and with low efficiency, it can be possible that an electron is transferred from P_{865} to BPheo* by HOMO-based electron transfer or, equivalently, HOMO-based hole transfer in the other direction (*65*−*68*), as is indicated in Figure 9b. This would then lead to a B-branch RP, $P^{\bullet+}_{865}\,H^{\bullet-}_B$, that can recombine to $^3P_{865}$ by the RP mechanism (see Figure 9b). The net result is that $^3P_{865}$ is formed after 537 nm excitation by a dominant isc mechanism and a minor contribution from a HOMO-based RP mechanism; the latter contribution is most prominently visible at the Y orientations. The latter mechanism implies charge separation in the HOMO instead of the LUMO, or "hole transfer", whereby the created hole in HOMO of the

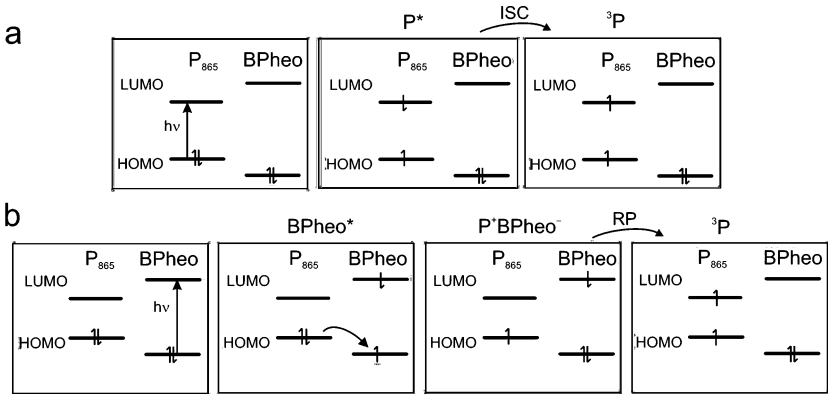

FIGURE 9: (a) Formation of $^3P_{865}$ at $T = 10$ K in *Rb. sphaeroides* LH(M214)/AW(M260) by the intersystem crossing (isc) mechanism at excitation of 865 nm; (b) possible HOMO-based formation of $^3P_{865}$ by the radical pair mechanism at excitation of 537 nm.

BPheo is filled by an electron from the donor. It is interesting to speculate whether both LUMO- and HOMO-based charge separation processes may occur under illumination by white (sun)light at room temperature under physiological conditions.

CONCLUSIONS

The observed polarization pattern at low temperature in the electron spin−echo detected EPR spectra of *Rb. sphaeroides* R-26.1, 2.4.1, and mutant GD(M203)/AW(M260) indicates that the triplet state of $^3P_{865}$ is formed via the radical pair mechanism. In mutant LH(M214)/AW(M260), the polarization pattern is completely different, and the triplet formation is explained by the isc mechanism. The observation of a $^3P_{865}$ signal formed by isc indicates the absence of long-lived radical pair precursor states along the A-branch. Also the native B-branch is not active in charge separation at $T = 10$ K. The situation changes when the temperature is raised to about 30 K. In the bRCs with carotenoid, triplet−triplet transfer $P_{865} \rightarrow$ Car is observed. Moreover, a contribution to the spectrum by the radical pair mechanism is observed in mutant LH(M214)/AW(M260), indicating that the B-branch is "switching on" at these temperatures. The observation that both the triplet−triplet energy transfer as well as the B-branch radical pair formation become active at the same temperature above about 30 K, and the observation that accessory bacteriochlorophyll on the B-branch is involved in both processes, we conclude that an energy barrier between the accessory bacteriochlorophyll and P_{865} exists that is overcome at temperatures above 30 K. The A-branch is operative even at 10 K in the native system, indicating that no thermal barrier exists for A-branch charge separation down to this temperature.

Second, a triplet carotenoid EPR signal has been observed above 30 K. The growth rate of this signal depends on the orientation of the reaction center in the magnetic field. The observed anisotropy of the growth rate can be traced back to that of the frequency associated with the radical pair precursor state $[P_{865}^{\bullet+}\ H^{\bullet-}]$ that oscillates between the singlet and triplet states with a frequency that depends on the orientation of the bRC in the magnetic field. This behavior is observed for both *Rb. sphaeroides* 2.4.1 and mutant GD(M203)/AW(M260), for which the quinone on the A-branch cannot occupy its normal binding pocket. It therefore seems that the presence of an additional spin on Q_A does not significantly influence the spin dynamics involved in the initial steps of charge separation.

Finally, small but significant changes in the electron spin−echo detected EPR spectrum of mutant LH(M214)/AW(M260) at 10 K have been observed upon change of the excitation wavelength to 537 nm. At this wavelength the remaining bacteriopheophytin in the B-branch is directly excited. The observed additional signals seem to stem from $^3P_{865}$ that is induced by a radical pair mechanism. A possible explanation for this observation is the existence of HOMO-based electron transfer, or hole transfer, in which the created hole on bacteriopheophytin is filled by an electron from P_{865} with concomitant formation of the B-branch $[P_{865}^{\bullet+}\ H_B^{\bullet-}]$ radical pair. All B-branch related processes observed in the EPR spectra at low temperature occur with an efficiency that is at most 1% of that of the corresponding processes of the A-branch. By the observations made here with EPR spectroscopy we conclude that this difference likely stems from a temperature-activated process between P_{865} and the accessory bacteriochlorophyll on the B-branch. A theoretical investigation as to what causes the difference between the rates of A and B-branch radical pair formation, e.g., with respect to the distance between P_{865} and the accessory bacteriochlorophylls of the A- and B-branches, is in progress.

ACKNOWLEDGMENT

The authors thank G. Schmitz (MPI BAC) for her help with the purification of reaction centers of *Rb. sphaeroides* R-26.1. Professors M. Y. Okamura, E. Abresch (UCSD), H. Selbach, and M. Reus (MPI BAC) are thanked for their help and kind advice at various stages of this project.

SUPPORTING INFORMATION AVAILABLE

ESE-detected triplet EPR spectra of $^3P_{865}$ in *Rb. sphaeroides* R-26.1 at different delay times between pulses at $T = 10$ K, simulation of EPR spectra, simulation of triplet formation, decay and transfer kinetics and two-dimensional DAF-EPR spectrum of $^3P_{865}$ in *Rb. sphaeroides* R-26.1 at $T = 10$ K. This material is available free of charge via the Internet at http://pubs.acs.org.

REFERENCES

1. Blankenship, B., Madigan, M., and Bauer, C. (1995) *Anoxygenic Photosynthetic Bacteria*, Kluwer Academic Publishers Dordrecht.

2. Thurnauer, M. C. (1979) ESR study of the photoexcited triplet state in photosynthetic bacteria, *Rev. Chem. Int. 100*, 197−231.
3. Allen, J. P., Feher, G., Yeates, T. O., Komiya, H., and Rees, D. C. (1987) Structure of the reaction center from *Rhodobacter sphaeroides* R-26—the cofactors, *Proc. Natl. Acad. Sci. U.S.A. 84*, 5730−5734.
4. Angerhofer, A. (1991) Chlorophyll triplets and radical pairs, in *Chlorophylls* (Scheer, H., Ed.) pp 945−991, CRC Press, Boca Raton, FL.
5. Feher, G., Allen, J. P., Okamura, M. Y., and Rees, D. C. (1989) Structure and function of bacterial photosynthetic reaction centers, *Nature 339*, 111−116.
6. Levanon, H., and Norris, J. R. (1978) Photoexcited triplet-state and photosynthesis, *Chem. Rev. 78*, 185−198.
7. Budil, D. E., and Thurnauer, M. C. (1991) The chlorophyll triplet-state as a probe of structure and function in photosynthesis, *Biochim. Biophys. Acta 1057*, 1−41.
8. Deisenhofer, J., Epp, O., Miki, K., Huber, R., and Michel, H. (1984) X-ray structure-analysis of a membrane-protein complex—electron-density map at 3A resolution and a model of the chromophores of the photosynthetic reaction center from *Rhodopseudomonas viridis*, *J. Mol. Biol. 180*, 385−398.
9. Michel, H. (1982) 3-Dimensional crystals of a membrane-protein complex—the photosynthetic reaction center from *Rhodopseudomonas viridis*, *J. Mol. Biol. 158*, 567−572.
10. Allen, J. P., Feher, G., Yeates, T. O., Komiya, H., and Rees, D. C. (1987) Structure of the reaction center from *Rhodobacter sphaeroides* R-26—the protein subunits, *Proc. Natl. Acad. Sci. U.S.A. 84*, 6162−6166.
11. Allen, J. P., Feher, G., Yeates, T. O., Komiya, H., and Rees, D. C. (1988) Structure of the reaction center from *Rhodobacter sphaeroides* R-26—protein cofactor (quinones and Fe-2+) interactions, *Proc. Natl. Acad. Sci. U.S.A. 85*, 8487−8491.
12. Yeates, T. O., Komiya, H., Chirino, A., Rees, D. C., Allen, J. P., and Feher, G. (1988) Structure of the reaction center from *Rhodobacter sphaeroides* R-26 and 2.4.1-protein-cofactor (bacteriochlorophyll, bacteriopheophytin, and carotenoid) interactions, *Proc. Natl. Acad. Sci. U.S.A. 85*, 7993−7997.
13. Volk, M., Aumeier, G., Langenbacher, T., Feick, R., Ogrodnik, A., and Michel-Beyerle, M. E. (1998) Energetics and mechanism of primary charge separation in bacterial photosynthesis. A comparative study on reaction centers of *Rhodobacter sphaeroides* and *Chloroflexus aurantiacus*, *J. Phys. Chem. B 102*, 735−751.
14. Borovykh, I. V., Proskuryakov, I. I., Klenina, I. B., Gast, P., and Hoff, A. J. (2000) Magnetophotoselection study of the lowest excited triplet state of the primary donor in photosynthetic bacteria, *J. Phys. Chem. B 104*, 4222−4228.
15. Paddock, M. L., Chang, C., Xu, Q., Abresch, E. C., Axelrod, H. L., Feher, G., and Okamura, M. Y. (2005) Quinone (Q(B)) reduction by B-branch electron transfer in mutant bacterial reaction centers from *Rhodobacter sphaeroides*: Quantum efficiency and X-ray structure, *Biochemistry 44*, 6920−6928.
16. de Boer, A. L., Neerken, S., de Wijn, R., Permentier, H. P., Gast, P., Vijgenboom, E., and Hoff, A. J. (2002) B-branch electron transfer in reaction centers of *Rhodobacter sphaeroides* assessed with site-directed mutagenesis, *Photosynth. Res. 71*, 221−239.
17. Wang, H. Y., Lin, S., Allen, J. P., Williams, J. C., Blankert, S., Laser, C., and Woodbury, N. W. (2007) Protein dynamics control the kinetics of initial electron transfer in photosynthesis, *Science 316*, 747−750.
18. Kirmaier, C., Laporte, L., Schenck, C. C., and Holten, D. (1995) The nature and dynamics of the charge-separated intermediate in reaction centers in which bacteriochlorophyll replaces the photoactive bacteriopheophytin .1. Spectral characterization of the transient state, *J. Phys. Chem. 99*, 8903−8909.
19. Kirmaier, C., Laporte, L., Schenck, C. C., and Holten, D. (1995) The nature and dynamics of the charge-separated intermediate in reaction centers in which bacteriochlorophyll replaces the photoactive bacteriopheophytin .2. The rates and yields of charge separation and recombination, *J. Phys. Chem. 99*, 8910−8917.
20. Heller, B. A., Holten, D., and Kirmaier, C. (1995) Control of electron-transfer between the L-side and M-side of photosynthetic reaction centers, *Science 269*, 940−945.
21. Haffa, A. L. M., Lin, S., Williams, J. C., Taguchi, A. K. W., Allen, J. P., and Woodbury, N. W. (2003) High yield of long-lived B-side charge separation at room temperature in mutant bacterial reaction centers, *J. Phys. Chem. B 107*, 12503−12510.
22. Lin, S., Katilius, E., Haffa, A. L. M., Taguchi, A. K. W., and Woodbury, N. W. (2001) Blue light drives B-side electron transfer in bacterial photosynthetic reaction centers, *Biochemistry 40*, 13767−13773.
23. de Boer, A. L., Neerken, S., de Wijn, R., Permentier, H. P., Gast, P., Vijgenboom, E., and Hoff, A. J. (2002) High yield of B-branch electron transfer in a quadruple reaction center mutant of the photosynthetic bacterium *Rhodobacter sphaeroides*, *Biochemistry 41*, 3081−3088.
24. Chuang, J. I., Boxer, S. G., Holten, D., and Kirmaier, C. (2006) High yield of M-side electron transfer in mutants of *Rhodobacter capsulatus* reaction centers lacking the L-side bacteriopheophytin, *Biochemistry 45*, 3845−3851.
25. Lubitz, W., Lendzian, F., and Bittl, R. (2002) Radicals, radical pairs and triplet states in photosynthesis, *Acc. Chem. Res. 35*, 313−320.
26. Ridge, J. P., van Brederode, M. E., Goodwin, M. G., van Grondelle, R., and Jones, M. R. (1999) Mutations that modify or exclude binding of the QA ubiquinone and carotenoid in the reaction center from *Rhodobacter sphaeroides*, *Photosynth. Res. 59*, 9−26.
27. McGann, W. J., and Frank, H. A. (1985) Transient electron-spin resonance spectroscopy of the carotenoid triplet-state in *Rhodopseudomonas sphaeroides* wild-type, *Chem. Phys. Lett. 121*, 253−261.
28. Hoff, A. J., and Proskuryakov, I. I. (1985) Triplet electron-paramagnetic-res spectra of the primary electron-donor in bacterial photosynthesis at temperatures between 15-K and 296-K, *Chem. Phys. Lett. 115*, 303−310.
29. Frank, H. A., Bolt, J. D., Costa, S. M. D. B., and Sauer, K. (1980) Electron-paramagnetic resonance detection of carotenoid triplet-states, *J. Am. Chem. Soc. 102*, 4893−4898.
30. Frank, H. A., Chynwat, V., Hartwich, G., Meyer, M., Katheder, I., and Scheer, H. (1993) Carotenoid triplet-state formation in *Rhodobacter sphaeroides* R-26 reaction centers exchanged with modified bacteriochlorophyll pigments and reconstituted with spheroidene, *Photosynth. Res. 37*, 193−203.
31. Hore, P. J. (1990) Analysis of polarized EPR spectra, in *Advanced EPR in Biology and Biochemistry* (Hoff, A., Ed.) pp 405−440, Elsevier, Amsterdam.
32. Feher, G., and Okamura, M. (1978) Chemical composition and properties of reaction centers, in *The Photosynthetic Bacteria* (Clayton, R. and Sistrom, W., Eds.) pp 349−386, Plenum Press, New York.
33. Frank, H. A., Friesner, R., Nairn, J. A., Dismukes, G. C., and Sauer, K. (1979) Orientation of the primary donor in bacterial photosynthesis, *Biochim. Biophys. Acta 547*, 484−501.
34. Lendzian, F., Bittl, R., and Lubitz, W. (1998) Pulsed ENDOR of the photoexcited triplet states of bacteriochlorophyll a and of the primary donor P-865 in reaction centers of *Rhodobacter sphaeroides* R-26, *Photosynth. Res. 55*, 189−197.
35. Plato, M., Möbius, K., Lubitz, W., Allen, J. P., and Feher, G. (1990) Magnetic resonance and molecular orbital studies of the primary donor states in bacterial reaction centers, in *Perspectives in Photosynthesis* (Jortner, J., and Pullman, B., Eds.) pp 423−434, Kluwer Academic Publishers, Dordrecht.
36. Lendzian, F., Endeward, B., Plato, M., Bumann, D., Lubitz, W., and Möbius, K. (1990) ENDOR and TRIPLE resonance investigation of the primary donor cation radical P865 in single crystals of *Rhodobacter sphaeroides* R-26 reaction centers, in *Reaction Centers of Photosynthetic Bacteria* (Michel-Beyerle, M. E., Ed.) pp 57−68, Springer-Verlag, Berlin.
37. Sinnecker, S., Reijerse, E., Neese, F., and Lubitz, W. (2004) Hydrogen bond geometries from electron paramagnetic resonance and electron-nuclear double resonance parameters: Density functional study of quinone radical anion−solvent interactions, *J. Am. Chem. Soc. 126*, 3280−3290.
38. Schweiger, A., and Jeschke, G. (2001) *Principles of Pulse Electron Paramagnetic Resonance*, Oxford University Press, Oxford.
39. Dauw, X. L. R., Poluektov, O. G., Warntjes, J. B. M., Bronsveld, M. V., and Groenen, E. J. J. (1998) Triplet-state dynamics of C-70, *J. Phys. Chem. A 102*, 3078−3082.
40. Ermler, U., Fritzsch, G., Buchanan, S. K., and Michel, H. (1994) Structure of the photosynthetic reaction-center from *Rhodobacter sphaeroides* at 2.65-angstrom resolution—cofactors and protein-cofactor interactions, *Structure 2*, 925−936.
41. Flanagan, H. L., and Singel, D. J. (1987) Analysis of N-14 Eseem patterns of randomly oriented solids, *J. Chem. Phys. 87*, 5606−5616.
42. Lucken, E. A. C. (1969) *Nuclear Quadrupole Coupling Constants*, Academic Press, London and New York.

43. Kosman, D. J., Peisach, J., and Mims, W. B. (1980) Pulsed electron-paramagnetic resonance studies of the copper(II) site in galactose-oxidase, *Biochemistry 19*, 1304−1308.
44. Mims, W. B., Peisach, J., Shaw, R. W., and Beinert, H. (1980) Electron-spin echo studies of cytochrome-*c* oxidase, *J. Biol. Chem. 255*, 6843−6846.
45. Mims, W. B., and Peisach, J. (1976) Assignment of a ligand in stellacyanin by a pulsed electron-paramagnetic resonance method, *Biochemistry 15*, 3863−3869.
46. Mondovi, B., Graziani, M. T., Mims, W. B., Oltzik, R., and Peisach, J. (1977) Pulsed electron-paramagnetic resonance studies of types-I and type-Ii copper of *Rhus-Vernicifera* laccase and porcine ceruloplasmin, *Biochemistry 16*, 4198−4202.
47. de Groot, A., Evelo, R., Hoff, A. J., de Beer, R., and Scheer, H. (1985) Electron-spin echo envelope modulation (Eseem) spectroscopy of the triplet-state of the primary donor of N-14 and N-15 bacterial photosynthetic reaction centers and of N-14 and N-15 bacteriochlorophyll-A, *Chem. Phys. Lett. 118*, 48−54.
48. Paschenko, S. V., Gast, P., and Hoff, A. J. (2001) A D-band (130 GHz) EPR study of the primary electron donor triplet state in photosynthetic reaction centers of *Rhodobacter sphaeroides* R-26, *Appl. Magn. Reson. 21*, 325−334.
49. Labahn, A., and Huber, M. (2001) The g-tensor anisotropy of the triplet state of the primary electron donor in the photosynthetic bacterium *Rhodobacter sphaeroides* by high-field (95 GHz) EPR, *Appl. Magn. Reson. 21*, 381−387.
50. Neese, F. (2006) Importance of direct spin-spin coupling and spin-flip excitations for the zero-field splittings of transition metal complexes: A case study, *J. Am. Chem. Soc. 128*, 10213−10222.
51. Frank, H. A., Chynwat, V., Posteraro, A., Hartwich, G., Simonin, I., and Scheer, H. (1996) Triplet state energy transfer between the primary donor and the carotenoid in *Rhodobacter sphaeroides* R-26.1 reaction centers exchanged with modified bacteriochlorophyll pigments and reconstituted with spheroidene, *Photochem. Photobiol. 64*, 823−831.
52. Kakitani, Y., Fujii, R., Koyama, Y., Nagae, H., Walker, L., Salter, B., and Angerhofer, A. (2006) Triplet-state conformational changes in 15-cis-spheroidene bound to the reaction center from *Rhodobacter sphaeroides* 2.4.1 as revealed by time-resolved EPR spectroscopy: Strengthened hypothetical mechanism of triplet-energy dissipation, *Biochemistry 45*, 2053−2062.
53. Angerhofer, A., Bornhauser, F., Aust, V., Hartwich, G., and Scheer, H. (1998) Triplet energy transfer in bacterial photosynthetic reaction centres, *Biochim. Biophys. Acta 1365*, 404−420.
54. Laible, P. D., Chynwat, V., Thurnauer, M. C., Schiffer, M., Hanson, D. K., and Frank, H. A. (1998) Protein modifications affecting triplet energy transfer in bacterial photosynthetic reaction centers, *Biophys. J. 74*, 2623−2637.
55. Angerhofer, A., and Aust, V. (1993) A monomeric bacteriochlorophyll triplet-state ((3)B) in reaction centers of *Rhodobacter sphaeroides* R-26, studied by absorption-detected magnetic-resonance, *J. Photochem. Photobiol., B 20*, 127−132.
56. Hartwich, G., Scheer, H., Aust, V., and Angerhofer, A. (1995) Absorption and Admr studies on bacterial photosynthetic reaction centers with modified pigments, *Biochim. Biophys. Acta 1230*, 97−113.
57. Hoff, A. J. (1976) Kinetics of populating and depopulating of components of photoinduced triplet-state of photosynthetic bacteria *Rhodospirillum rubrum*, *Rhodopseudomonas spheroides* (wild-type), and its mutant R-26 as measured by ESR in zero-field, *Biochim. Biophys. Acta 440*, 765−771.
58. Clarke, R. H., Connors, R. E., Schaafsma, T. J., Kleibeuker, J. F., and Platenkamp, R. J. (1976) Triplet-state of chlorophylls, *J. Am. Chem. Soc. 98*, 3674−3677.
59. Metz, F. (1973) Position-dependent deuterium effect on relative rate constants for Isc processes in aromatic-hydrocarbons, *Chem. Phys. Lett. 22*, 186−190.
60. Monger, T. G., Cogdell, R. J., and Parson, W. W. (1976) Triplet-states of bacteriochlorophyll and carotenoids in chromatophores of photosynthetic bacteria, *Biochim. Biophys. Acta 449*, 136−153.
61. Bittl, R., van der Est, A., Kamlowski, A., Lubitz, W., and Stehlik, D. (1994) Time-resolved Epr of the radical pair P(865)(+)Q(A)(-) in bacterial reaction centers—observation of transient nutations, quantum beats and envelope modulation effects, *Chem. Phys. Lett. 226*, 349−358.
62. Arnoux, B., Ducruix, A., Reisshusson, F., Lutz, M., Norris, J., Schiffer, M., and Chang, C. H. (1989) Structure of spheroidene in the photosynthetic reaction center from Y-*Rhodobacter-sphaeroides*, *FEBS Lett. 258*, 47−50.
63. Woodbury, N., and Allen, J. (1995) in *Anoxygenic Photosynthetic Bacteria* (Blankenship, R., Madigan, M., and Bauer, C., Eds.) Kluwer Academic Publishers, Dordrecht, The Netherlands.
64. Bixon, M., Jortner, J., Michel-Beyerle, M. E., and Ogrodnik, A. (1989) A superexchange mechanism for the primary charge separation in photosynthetic reaction centers, *Biochim. Biophys. Acta 977*, 273−286.
65. Allen, G. C., and Hush, N. S. (1967) Reflectance spectrum and electronic states of CuCl ion in a number of crystal lattices, *Inorg. Chem. 6*, 4−15.
66. Osuka, A., Mataga, N., and Okada, T. (1997) A chemical approach towards the photosynthetic reaction center, *Pure Appl. Chem. 69*, 797−802.
67. Reimers, J. R., and Hush, N. S. (2004) Unified description of the electrochemical, charge distribution, and spectroscopic properties of the special-pair radical cation in bacterial photosynthesis, *J. Am. Chem. Soc. 126*, 4132−4144.
68. Breton, J., Nabedryk, E., and Parson, W. W. (1992) A new infrared electronic-transition of the oxidized primary electron-donor in bacterial reaction centers—a way to assess resonance interactions between the bacteriochlorophylls, *Biochemistry 31*, 7503−7510.

BI701593R